The effects of crystallographic orientation and strain on the properties of excitonic emission from wurtzite InGaN/GaN quantum wells

S Khatsevich and D H Rich

Department of Physics, The Ilse Katz Institute for Nanoscience and Nanotechnology,
Ben-Gurion University of the Negev, POB 653, Beer-Sheva 84105, Israel

Abstract
We have examined in detail crystal orientation effects on the properties of excitonic emission from wurtzite $In_xGa_{1-x}N$/GaN quantum wells (QWs) with piezoelectric polarization using exciton binding and transition energy calculations based on a single-band effective-mass theory. We show numerical results for the bandgaps, effective heavy-hole masses, piezoelectric polarizations and fields, exciton wavefunctions, exciton binding and transition energies and radiative lifetimes of excitonic emission as a function of the QW crystallographic growth planes. Band-edge and effective-mass parameters for a continuum of GaN crystallographic orientations, on which InGaN/GaN QWs are grown, were obtained from In-composition- and strain-dependent $\mathbf{k} \cdot \mathbf{p}$ calculation for wurtzite $In_xGa_{1-x}N$, using the 6×6 $\mathbf{k} \cdot \mathbf{p}$ Hamiltonian in appropriate $\{hkil\}$ representations. We have performed calculations for a continuum of technologically relevant QW growth planes $\{h\bar{h}0l\}$ oriented at various angles θ relative to the (0001) c-plane. The excitonic ground- and first-excited-state energies and wavefunctions were calculated using an effective potential method. A strong reduction of average in-plane heavy-hole effective mass and normal to the plane piezoelectric polarization and field is observed as θ varies from $\theta = 0°$ (i.e. the c-axis direction) to $\theta = 49.5°$, where the piezoelectric polarization and electric field reverse their orientation with respect to the plane of the QW. The decrease of the electric field in the InGaN/GaN QW growth direction leads to an increased exciton transition energy and oscillator strength, which results in the increase of the exciton binding energy and decrease of the excitonic radiative lifetime. For angles $\theta > 49.5°$ only small variations on the order of ~10% in the exciton binding and transition energies and excitonic radiative lifetime are observed for narrow $In_{0.12}Ga_{0.88}N$/GaN QWs that have widths less than ~ 3.5 nm. The average in-plane heavy-hole effective mass reaches its minimum for $\theta = 90°$, i.e. m-plane $\{1\bar{1}00\}$ growth. These results indicate that InGaN/GaN QW structures grown on non-(0001)-oriented planes in a wide variety of angles $49.5° \leqslant \theta \leqslant 90°$ can be used for optimized operation of optoelectronic devices.

1. Introduction

In recent years, much attention has been paid to a new class of low-dimensional structures, made of hexagonal (wurtzite) group III nitride semiconductors. $In_xGa_{1-x}N$/GaN single quantum wells (SQWs) and multiple quantum wells (MQWs) have been studied intensively both experimentally and theoretically due to their potential applications for the production of efficient optoelectronic devices, such as light emitting diodes (LEDs) [1, 2] and laser diodes (LDs) [3] that can emit in the blue/violet spectral region. The efficiency of LEDs and LDs, which contain the InGaN QW materials grown on the c-plane in their active region, suffers from large strain induced piezoelectric [4–6] and spontaneous polarizations [5, 6], which lead to large electric fields in the strained layers. Many studies have reported the important

role of the large internal electric field in InGaN QWs [5], comparable to or much larger than ~1 MV cm^{-1} for QWs grown on the c-plane, which induces a large redshift in the transition energies [7, 8] due to the quantum confined Stark shift effect (QCSE) [8–10] and attendant reduction in the oscillator strength [8, 10, 11] owing to the field-induced separation of the electron and hole wavefunctions towards the opposite sides of the QW.

Recently, growth on non-[0001]-oriented crystal planes has been considered as one of the possible ways to create more favorable parameters for LEDs and LDs. While good crystalline quality can be achieved for c-plane growth of InGaN/GaN QWs, the quantum efficiency of LEDs decreases with increasing wavelength, resulting partially from the reduced oscillator strength associated with the field-induced separation of electrons and holes [12]. Thus, it is advantageous to grow InGaN/GaN QWs on crystallographic surfaces that will enable a significant reduction or even a complete elimination of the internal field. Such goals have supplied the impetus for the growth of heterostructures on the non-polar (11$\bar{2}$0) a-plane through growth of GaN on the r-plane of sapphire [13–15], as well as for the growth of non-polar (1$\bar{1}$00) m-plane GaN by growing on more uncommon substrates, such as LiAlO$_2$ [16]. The crystalline quality of the GaN growth on more exotic substrates still lags behind that of the more conventionally grown c-plane sapphire or SiC wafers, as non-polar GaN faces currently suffer from a high density of threading dislocations and stacking faults [16]. Sufficient motivation consequently exists to seek a compromise between a reduced piezoelectric field and defect density in order to attain an acceptable balance between the radiative and nonradiative lifetimes for an enhanced quantum efficiency. Thus, other approaches involve the selective growth of semi-polar side facets such as {1$\bar{1}$01} on c-plane GaN substrates and the subsequent growth of semi-polar InGaN/GaN heterostructures for the purpose of LEDs and lasers with high efficiency [17–20]. Recently, the successful fabrication of blue LEDs was demonstrated by InGaN/GaN QW growth on semi-polar faces of (10$\bar{1}\bar{1}$) and (10$\bar{1}\bar{3}$) [21], as well as for the growth of blue, green and amber LEDs on the semi-polar {11$\bar{2}$2} faces [22]. Likewise, the successful growth of blue LEDs was also achieved on the non-polar GaN (1$\bar{1}$00) m-plane [23]. A direct measurement of the electric field in InGaN QWs grown on semi-polar (1$\bar{1}$01) facets has been performed and yielded a field of ~0.1 MV cm^{-1}, in comparison to a measured value of 1.9 MV cm^{-1} for similar QWs grown on the c-plane [24].

The influence of crystal orientation on the electronic and optical properties of wurtzite GaN and InGaN/GaN QW structures has been studied theoretically using the multiband effective-mass theory [25, 26]. These works showed that several important properties such as the piezoelectric and spontaneous polarizations, transition energy, transition probability, and effective mass depend strongly on the crystal orientation. In particular, the electric fields are largest in the most commonly used [0001] c-plane growth direction [27, 28] and are expected to be
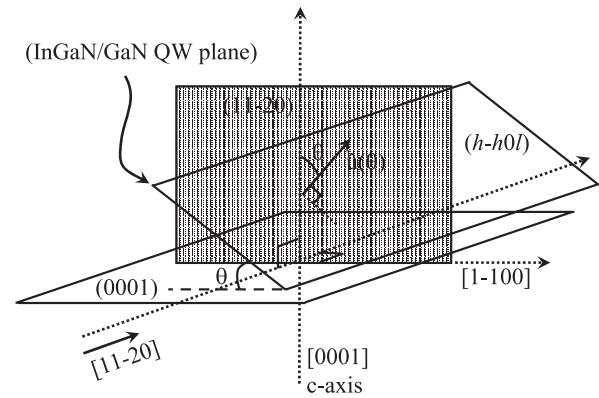

Figure 1. Schematic diagram showing the geometry of the family of {$hh0l$} planes and the InGaN/GaN QW growth direction $\hat{\mathbf{u}}(\theta)$ for which the various calculations of piezoelectric field, exciton binding energy, transition energy and radiative lifetime are performed.

zero for the [1$\bar{1}$00] m-plane growth direction [25, 26], which makes an angle of 90° with the c-axis. Although excitonic effects are significant in wurtzite InGaN/GaN QW materials grown on non-[0001]-oriented planes even at room temperature [29, 30], these effects have been vastly neglected in previous works [25, 26]. Feneberg and Thonke have recently calculated the piezoelectric polarizations, fields, and transition energies for In$_x$Ga$_{1-x}$N/GaN QWs with varying compositions x, carrier densities, and growth directions [31].

In this paper, we build upon previous studies by using a single-band effective-mass approximation in order to examine crystal orientation effects on the properties of excitonic emission from InGaN/GaN QW structures which include exciton binding energies, transition energies and radiative lifetimes of free and strongly localized excitons. We present numerical results for the bandgaps, effective heavy-hole masses, piezoelectric polarizations and fields, exciton wavefunctions, exciton binding and transition energies, and excitonic radiative lifetimes as a function of the QW growth direction, $\hat{\mathbf{u}}(\theta)$, which is normal to the plane of the QW. We have performed such calculations for a continuum of technologically relevant QW growth planes {$h\bar{h}0l$} oriented at various angles θ relative to the (0001) c-plane, as schematically illustrated in figure 1. Band-edge and effective-mass parameters for a given QW growth direction $\hat{\mathbf{u}}(\theta)$ were first obtained from In-composition-and strain-dependent $\mathbf{k} \cdot \mathbf{p}$ calculations for wurtzite In$_x$Ga$_{1-x}$N, using a 6×6 $\mathbf{k} \cdot \mathbf{p}$ Hamiltonian in the appropriate {$hkil$} representation. We then calculated the exciton binding energies, E_B, by substitution of respective single electron and hole envelope wavefunctions for an appropriate QW growth direction, computed by solutions to the Schrödinger equation for a particle subject to an electric field, into a radial eigenvalue equation that involves the electron–hole relative motion in an effective in-plane Coulomb potential. These theoretical calculations are expected to help provide fundamental parameters, insights and clues for the future design of suitable growth orientations and structures for efficient polar, semi-polar, and non-polar In$_x$Ga$_{1-x}$N/GaN optoelectronic devices.
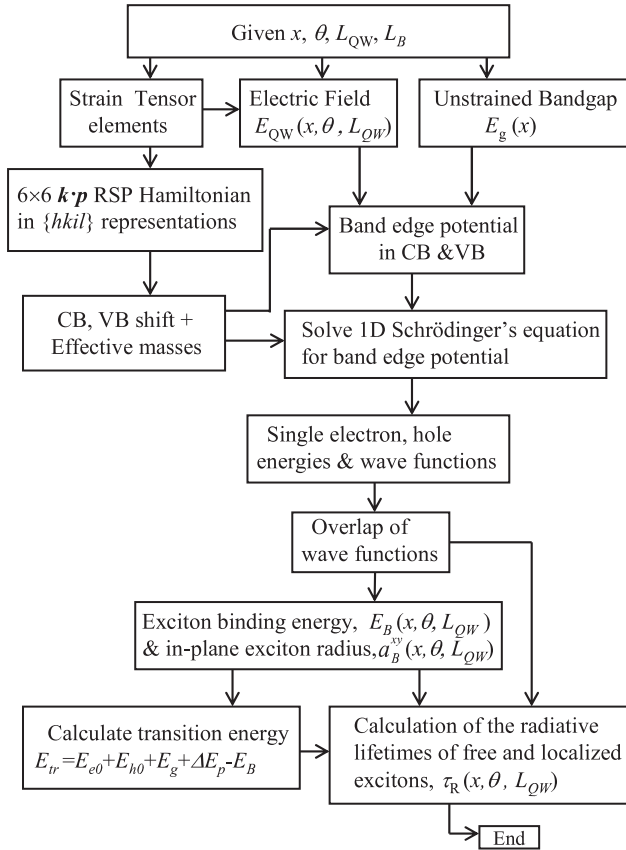
Figure 2. Flow chart illustrating the details of the model calculations of the exciton binding and transition energies, the in-plane Bohr radius and excitonic radiative lifetimes as a function of InGaN/GaN QW growth direction and width.

2. Modeling approach

In order to model orientation-dependent variations in the exciton binding and transition energies, the in-plane exciton radius and radiative lifetimes of excitonic emission, we have employed a single-band effective-mass approximation in the calculation of the electron and hole eigenstates of the $In_xGa_{1-x}N/GaN$ QWs. The block diagram illustrating the model calculation is shown in figure 2. For a given In composition and QW growth direction, $\hat{\mathbf{u}}(\theta)$, we have employed a full $\mathbf{k} \cdot \mathbf{p}$ perturbation method, that is appropriate for strained wurtzite $In_xGa_{1-x}N$ to calculate the bulk valence band dispersions and hole effective masses for dispersion along an appropriate $[hkil]$ direction [25, 26]. The relevant parameters in the $\mathbf{k} \cdot \mathbf{p}$ method for a wurtzite crystal include the A_i, which are similar to the Luttinger parameters in a zinc-blende crystal; the D_i, which are the deformation potentials for the $In_xGa_{1-x}N$ layers; c_{ij}, the elastic constants, and ε_{ij}, the strain tensor, which is appropriate for QWs pseudomorphically grown on the $(hkil)$ planes [25]. The $\mathbf{k} \cdot \mathbf{p}$ calculation was performed by transforming the 6×6 Hamiltonian for the valence band structure in the wurtzite crystal from the (0001) orientation into the appropriate strain-dependent Hamiltonian for a biaxial stress in the $\{hkil\}$ plane. In particular, as mentioned above, we will direct our calculations for the family

of $\{h\bar{h}0l\}$ planes whose normal is represented by $\hat{\mathbf{u}}(\theta)$. The $\mathbf{k} \cdot \mathbf{p}$ parameters for $In_xGa_{1-x}N$ were obtained by linearizing between those for InN and GaN for a given composition x. All numerical parameters that were employed in our $\mathbf{k} \cdot \mathbf{p}$ and polarization calculations are available in [29]. After a determination of the valence band energy dispersions for a given In composition, the heavy-hole effective masses, m_{hh}^z, for dispersion along the QW growth direction $\hat{\mathbf{u}}(\theta)$ (i.e. as also denoted by the z-Cartesian coordinate) and the average in-plane effective masses, m_{hh}^x and m_{hh}^y, were determined. The electron effective masses for dispersion in the QW x–y plane and along the QW z-direction were obtained by a linearization between values for InN and GaN as $m_e^{xy} = (0.23–0.13x)m_0$ and $m_e^z = (0.19–0.08x)m_0$ [29]. Note that we define the x, y, z crystallographic directions for c-plane growth in the usual manner as $[1\bar{1}00]$, $[11\bar{2}0]$, and $[0001]$, respectively. The conduction to valence band offset in wurtzite $In_xGa_{1-x}N$ is assumed to be independent of x, and is taken as $\Delta E_c/\Delta E_v = 70/30$, as has been proposed recently by different researchers [32–34]. We take the unstrained $In_xGa_{1-x}N$ bandgap at an arbitrary temperature as [35, 36]

$$E_g^{In_xGa_{1-x}N}(T) = E_g^{In_xGa_{1-x}N}(0) - \frac{10^{-3}T^2}{(1196 + T)},$$
$$E_g^{In_xGa_{1-x}N}(0) = 0.7x + 3.5(1 - x) - 2.72x(1 - x),$$

(1)

where $E_g^{In_xGa_{1-x}N}(0)$ is the unstrained $In_xGa_{1-x}N$ bandgap at $T = 0$ K [36]. The strain induced variation in the bandgap, which depends on the $In_xGa_{1-x}N$ crystal orientation, is given by solutions from the $\mathbf{k} \cdot \mathbf{p}$ calculations which included the deformation potentials for a particular strain tensor. The piezoelectric tensor elements, d_{ijk}, and spontaneous polarization parameter, P_{sp}, were also used to calculate the electric field in the QW and barriers, E_{QW} and E_B, for an arbitrary QW growth direction, as will be discussed in more detail in section 2.1.

Single particle electron and hole envelope wavefunctions in the QW growth direction, $\eta_{e,h}(z_{e,h})$, and ground-state energies were determined by solutions to the Schrödinger equation for a particle subject to an electric field, using a finite-element technique that was modified for the case of variable effective masses [37–39]. We have then solved for the ground-state wavefunction and binding energy of Wannier excitons, E_B, which are assumed to be formed by electrons and holes in the $In_xGa_{1-x}N/GaN$ QW, by substitution of the respective single particle electron and hole wavefunctions into a radial eigenvalue equation that involves the electron–hole relative motion in an effective in-plane Coulomb potential, as will be discussed in more detail in section 2.2 [40].

2.1. Calculation of energy-band structures and piezoelectric polarizations for various InGaN/GaN QW growth directions

The band structure near the direct band edges at $k = 0$ has the largest influence on most of the electronic and optical properties. Since the mixing of conduction and valence bands near the direct band edges is negligible, due to large energy separation, the exact 8×8 $\mathbf{k} \cdot \mathbf{p}$ Hamiltonian obtained from the

3

Kane model for wurtzite semiconductors can be simplified to 6×6 **k·p** Hamiltonian for the valence band structure, i.e., the so called Rashba–Sheka–Pikus (RSP) Hamiltonian [41, 42]. The RSP Hamiltonian can be derived using **k·p** perturbation theory and group theory arguments [42]. This effective-mass Hamiltonian is usually written in a choice of basis functions such that the z-axis coincides with the [0001] lattice growth orientation (c-axis). The frequently used basis is given by the inner product of $|l, m\rangle|1/2, s\rangle$, with $l = 1$, $m = 0, \pm 1$ and $s = \pm 1/2$. The basis states are expressed explicitly as follows [42]:

$$|u_1\rangle = |u_{hh \uparrow}\rangle = -\frac{1}{\sqrt{2}}|(X + iY) \uparrow\rangle,$$

$$|u_2\rangle = |u_{lh \uparrow}\rangle = \frac{1}{\sqrt{2}}|(X - iY) \uparrow\rangle,$$

$$|u_3\rangle = |u_{sh \uparrow}\rangle = |Z \uparrow\rangle,$$

$$|u_4\rangle = |u_{hh \downarrow}\rangle = \frac{1}{\sqrt{2}}|(X - iY) \downarrow\rangle, \quad (2)$$

$$|u_5\rangle = |u_{lh \downarrow}\rangle = -\frac{1}{\sqrt{2}}|(X + iY) \downarrow\rangle,$$

$$|u_6\rangle = |u_{sh \downarrow}\rangle = |Z \uparrow\rangle,$$

where the sub-indices hh, lh, and sh denote heavy, light, and split-off holes, respectively. In this basis the strained RSP Hamiltonian is nearly block diagonal. The full RSP Hamiltonian for a [0001]-oriented wurtzite crystal in the presence of strain takes the form [42]

$$H(k, \varepsilon)$$
$$= \begin{pmatrix} F & -K^* & -H^* & 0 & 0 & 0 \\ -K & G & H & 0 & 0 & \sqrt{2}\Delta_3 \\ -H & H^* & \lambda & 0 & \sqrt{2}\Delta_3 & 0 \\ 0 & 0 & 0 & F & -K & H \\ 0 & 0 & \sqrt{2}\Delta_3 & -K^* & G & -H^* \\ 0 & \sqrt{2}\Delta_3 & 0 & H^* & -H & \lambda \end{pmatrix}, \quad (3)$$

where

$$F = \Delta_1 + \Delta_2 + \lambda + \theta,$$

$$G = \Delta_1 - \Delta_2 + \lambda + \theta,$$

$$\lambda = \frac{\hbar^2}{2m_0}[A_1 k_z^2 + A_2(k_x^2 + k_y^2)] + \lambda_\varepsilon,$$

$$\theta = \frac{\hbar^2}{2m_0}[A_3 k_z^2 + A_4(k_x^2 + k_y^2)] + \theta_\varepsilon,$$

$$K = \frac{\hbar^2}{2m_0}A_5(k_x + ik_y)^2 + D_5\varepsilon_+, \quad (4)$$

$$H = \frac{\hbar^2}{2m_0}A_6(k_x + ik_y)k_z + D_6\varepsilon_{z+},$$

$$\lambda_\varepsilon = D_1\varepsilon_{zz} + D_2(\varepsilon_{xx} + \varepsilon_{yy}),$$

$$\theta_\varepsilon = D_3\varepsilon_{zz} + D_4(\varepsilon_{xx} + \varepsilon_{yy}),$$

$$\varepsilon_+ = \varepsilon_{xx} - \varepsilon_{yy} + 2i\varepsilon_{xy},$$

$$\varepsilon_{z+} = \varepsilon_{xz} + i\varepsilon_{yz},$$

where k_i is the wavevector, ε_{ij} the strain tensor, Δ_1 is the crystal-field split energy, and Δ_2 and Δ_3 characterize the energy shifts of the valence band structure induced by the spin–orbit interactions, $\Delta_1 = \Delta_{cr}$, $\Delta_2 = \Delta_3 = (1/3)\Delta_{so}$. The A_i are the valence band effective-mass parameters, which are similar to the Luttinger parameters in a zinc-blende crystal, and the D_i are the Bir–Picus deformation potentials for wurtzite crystals, which are similar to the hydrostatic a and uniaxial b deformation potentials in zinc-blende materials [42]. The order of the basis in the RSP Hamiltonian is as indicated by the sequential list of Bloch states in equation (2). The strained 6×6 RSP Hamiltonian for an arbitrary wurtzite crystal orientation can be obtained by substituting the transformation relation for the vector $\vec{k}$ and the strain elements for a general crystal orientation into the RSP Hamiltonian for the [0001] c-axis orientation, determined by equation (3) [42, 43]. The relation between the coordinate systems for vectors and tensors is expressed as [44]

$$k_i' = \sum_\alpha U_{i\alpha}k_\alpha,$$

$$\varepsilon_{ij}' = \sum_{\alpha\beta} U_{i\alpha}U_{j\beta}\varepsilon_{\alpha\beta}, \quad (5)$$

$$c_{ijkl}' = \sum_{\alpha\beta\gamma\delta} U_{i\alpha}U_{j\beta}U_{k\gamma}U_{l\delta}c_{\alpha\beta\gamma\delta}$$

where summations over repeated indices are indicated. Here U is a rotation matrix that transforms the physical quantities from (x, y, z) coordinates to (x', y', z') coordinates, where the z-axis corresponds to the c-axis [0001] and the z'-axis is parallel to $\hat{u}(\theta)$ and normal to the QW growth plane [17, 43].

$$U = \begin{pmatrix} \cos\theta & 0 & -\sin\theta \\ 0 & 1 & 0 \\ \sin\theta & 0 & \cos\theta \end{pmatrix}. \quad (6)$$

The polar angle θ is defined as the angle between the growth direction $\hat{u}(\theta)$ and the c-axis, as illustrated in figure 1. The strain tensor elements in the (x, y, z) coordinates for a general crystal plane $\{hkil\}$ are determined from the condition that the layer is grown pseudomorphically, and these strain elements should minimize the strain energy of the layer simultaneously [45, 46]. After block-diagonalization of the transformed 6×6 **k·p** RSP Hamiltonian, the dispersion relations in the valence band $E_{hh}(\vec{k}')$, $E_{lh}(\vec{k}')$ and $E_{ch}(\vec{k}')$ can be determined.

For an arbitrary InGaN/GaN QW growth direction the electric fields in the well and barriers, which appear due to the piezoelectric (PZ) and spontaneous (SP) polarizations normal to the QW plane, can be estimated from (i) the periodic boundary condition for the superlattice structure and (ii) the assumption that the dielectric displacement field is conserved along the growth axis [27, 47]

$$E_w = E_w^{sp} + E_w^{pz} = \frac{L_B(P_B^{sp} - P_w^{sp})}{\varepsilon_0(\varepsilon_B L_w + \varepsilon_w L_B)} - \frac{L_B P_w^{pz}}{\varepsilon_0(\varepsilon_B L_w + \varepsilon_w L_B)}$$

$$E_B = -E_w\frac{L_w}{L_B}, \quad (7)$$

where subscripts w and B denote the well and barrier, respectively, and L and ε are the layer width and static dielectric constant, respectively. The normal piezoelectric polarization with respect to the growth plane for an arbitrary QW growth direction, $P_z'^{pz}$, can be expressed as [43]

$$P_z'^{pz} = P_x^{pz} \sin\theta + P_z^{pz} \cos\theta, \tag{8}$$

where the polarization components along the x and z axes, P_x^{pz} and P_z^{pz}, are given by

$$P_x^{pz} = 2d_{15}c_{44}\varepsilon_{xz},$$
$$P_z^{pz} = [d_{31}(c_{11} + c_{12}) + d_{33}c_{13}](\varepsilon_{xx} + \varepsilon_{yy}) \tag{9}$$
$$+ [2d_{31}c_{13} + d_{33}c_{33}]\varepsilon_{zz}.$$

2.2. Calculation of the orientation-dependent exciton binding and transition energies and excitonic radiative lifetimes in wurtzite InGaN/GaN QWs

Within the effective-mass approximation, the exciton Hamiltonian in a QW can be written as [48]

$$H = \frac{p_{ze}^2}{2m_e} + \frac{p_{zh}^2}{2m_h} + \frac{P_X^2 + P_Y^2}{2(m_e + m_h)} + \frac{p_x^2 + p_y^2}{2\mu}$$
$$+ V_e(z_e) + V_h(z_h) - \frac{e^2}{\varepsilon\sqrt{x^2 + y^2 + (z_e - z_h)^2}}, \tag{10}$$

with

$$(m_e + m_h)\vec{R} = m_e\vec{r}_e + m_h\vec{r}_h, \qquad \vec{r} = \vec{r}_e - \vec{r}_h$$

where $\vec{P}$ is the center-of-mass momentum, $V_e(z_e)$ and $V_h(z_h)$ are the quantum well potentials for electrons and holes, respectively, ε is the relative dielectric constant and μ is the reduced electron–hole mass in the layer plane. An exact solution of equation (10) is clearly not possible. The approximate solutions of this problem are based on using trial wavefunctions of the form [48–50]

$$\Psi(r, z_e, z_h) = \eta_e(z_e)\eta_h(z_h)\Phi_{e-h}(r, z_e - z_h), \tag{11}$$

where $\eta_e(z_e)$ and $\eta_h(z_h)$ are the single particle envelope wavefunctions that describe the motion of electrons and holes in the QW growth direction, while $\Phi_{e-h}(r, z_e - z_h)$ describes the relative in-plane electron–hole motion. Within the effective-mass approximation, omitting the center-of-mass kinetic energy of the in-plane electron and hole motion, the exciton Hamiltonian in a QW can be written in the following form [48]:

$$H^* = H_{ez} + H_{hz} + H_{eh}, \qquad \text{where}$$

$$H_{ez} = -\frac{\hbar^2}{2m_e}\frac{d^2}{dz_e^2} + V_e(z_e),$$

$$H_{hz} = -\frac{\hbar^2}{2m_h}\frac{d^2}{dz_h^2} + V_h(z_h), \tag{12}$$

$$H_{ez} = -\frac{\hbar^2}{2\mu}\frac{d^2}{dr^2} - \frac{e^2}{\varepsilon\sqrt{x^2 + y^2 + (z_e - z_h)^2}}.$$

Most of the previous studies employed a variational approach to get an estimation of the exciton binding energy and Bohr radius [48–50]. However, the success of the variational method relies heavily upon the choice of the trial function, and the criteria for the choice depend on the particular problem and cannot easily be generalized. We calculate the exciton binding energies, the in-plane wavefunctions and the in-plane exciton radius using an effective potential method [40]. To simplify the situation we use a simple trial wavefunction of the form

$$\Psi(r, z_e, z_h) = \eta_e(z_e)\eta_h(z_h)\Phi_{e-h}(r), \tag{13}$$

where $\Phi_{e-h}(r)$ describes the relative in-plane electron–hole motion and is assumed to depend only on the in-plane relative coordinate r for the purpose of separating variables. With the above assumptions, the eigenvalue equation of the exciton Hamiltonian described in equation (12) can be reduced to the following radial equation for the exciton binding energy [40]:

$$-\frac{\hbar^2}{2\mu}\frac{1}{r}\frac{d}{dr}\left(r\frac{d}{dr}\right)\Phi_{e-h}(r) + V(r)\Phi_{e-h}(r) = -E\Phi_{e-h}(r), \tag{14}$$

where $V(r)$ is the effective in-plane Coulomb potential defined by

$$V(r) = -\frac{e^2}{\varepsilon}\int dz_e \int dz_h \frac{|\eta_e(z_e)|^2|\eta_h(z_h)|^2}{\sqrt{r^2 + (z_e - z_h)^2}}. \tag{15}$$

A detailed description of this potential function, including its derivation, and calculated shape using a form factor method, is presented in [40].

It is easy to derive the required boundary conditions for the eigenfunction Φ_{e-h} at the origin, namely $d\Phi_{e-h}(z)/dz = 0$ for $z = 0$, and with a trivial boundary condition at infinity the problem for exciton eigenvalues and eigenfunctions can be set as

$$\frac{d^2}{dr^2}\Phi_{e-h}(r) + \frac{1}{r}\frac{d}{dr}\Phi_{e-h}(r) - \frac{2\mu}{\hbar^2}(V(r) - E)\Phi_{e-h}(r) = 0,$$

$$\frac{d\Phi_{e-h}(r)}{dr}\bigg|_{r=0} = 0,$$

$$\Phi_{e-h}(r)|_{r\to\infty} \to 0. \tag{16}$$

The reduction of the 3D problem of the excitonic wavefunction to this 1D exciton eigenvalue problem, using the trial wavefunctions of equations (11) and (13), is generally valid and accurate for quantum wells for which the barrier heights are much larger than the effective Rydberg of the system [40]. This is certainly true for the present case of $In_xGa_{1-x}N/GaN$ QWs with $x \approx 0.12$ in which the total effective QW barrier heights are a few hundred meV and much larger than the exciton binding energy, which is less than $\sim$40 meV (as will be shown in section 3) [29].

We solved numerically equation (16), using the method of finite differences. To ensure sufficient numerical accuracy, we choose a large, but finite, value of the cutoff r_c and assume that the exciton wavefunctions are identically zero for $r = r_c$. To avoid the problem of a singularity for the function $V(r)$ at the origin, we begin the numerical integration from $r_0 = \varepsilon_1$, where

ε_1 can be made arbitrary small to ensure numerical accuracy. As a result of the spread of the carrier wavefunctions in the z direction, the Coulomb interaction is greatly reduced for small in-plane x, y distances, and this also partially justifies the current approach. For a known ground-state wavefunction $\Phi_{0(e-h)}$ the in-plane exciton radius can be estimated as [48]

$$a_B^{xy} = \left(\Delta_r \sum_{i=1}^{N} \Phi_{i0} r_i^2 \Phi_{i0}^* \right)^{1/2}. \qquad (17)$$

We calculate the exciton transition energies in the QW as

$$E_{tr} = E_e + E_h + E_g + \Delta E_p - E_B, \qquad (18)$$

where E_e and E_h are eigenvalues of the 1D Schrödinger equation for a particle (electron or hole) subject to an electric field, E_g is the fundamental energy bandgap of the unstrained $In_x Ga_{1-x}N$ bulk material, ΔE_p is the strain induced variation in the bandgap and E_B is the exciton binding energy. In order to calculate excitonic radiative lifetimes of free and strongly bound excitons we used an approach that is described elsewhere [51, 52].

3. Numerical results and discussion

3.1. Crystal orientation effects on the energy-band structure and piezoelectric polarization

Figure 3 shows calculated valence band dispersion relations obtained by solutions of the 6×6 **k · p** RSP Hamiltonian for $In_{0.12}Ga_{0.88}N$/GaN QWs with the following growth planes: (a) (0001) ($\theta = 0°$) and (b) ($1\bar{1}01$) (i.e., $\hat{\mathbf{u}}(\theta)$ is such that $\theta = 62°$). Heavy-hole (HH), light-hole (LH) and crystal-field split-off hole (CH) band dispersions are indicated. For the (0001) c-plane, a symmetric in-plane k_x–k_y band profile is found, as observed in figure 3(a). The lattice mismatch between the epilayer ($In_{0.12}Ga_{0.88}N$) and the substrate (GaN) leads to a biaxial compressive strain of $\varepsilon_{xx} = \varepsilon_{yy} = -0.013$, as indicated. Dramatic changes are observed for QW growth on the ($1\bar{1}01$) plane, as seen in figure 3(b). The dissimilar warping of valence bands along the k_x' and k_y' axes results in a band profile asymmetric in the k_x'–k_y' plane. The inset in figure 3 shows the strain tensor elements as a function of angle θ between the $In_{0.12}Ga_{0.88}N$ QW growth direction and the [0001] c-axis direction. For $\theta > 0$, a strong modification of the strain tensor elements is observed so that $\varepsilon_{xx} \neq \varepsilon_{yy}$. Note that the component ε_{yy} is constant and the component ε_{xz} is zero for the [0001] growth direction ($\theta = 0$). The absolute values of the strain components ε_{xx} and ε_{zz} reach a maximum for $\theta = 90°$.

The effect of crystal orientation on the valence band-edge energies at $k = 0$ is shown in figure 4(a) for $In_{0.12}Ga_{0.88}N$/GaN QWs. For $\theta > 0$, the strain induced shift is positive for the HH and LH and negative for the CH band edges. The absolute values of the strain induced shift of HH and CH band edges increase with angle θ and reach a maximum at $\theta = 35°$ for the HH band and at $\theta = 38°$ for the CH band. For the LH band, the strain induced shift is positive and its absolute value is increasing with angle θ in the $0 < \theta \leqslant 68°$
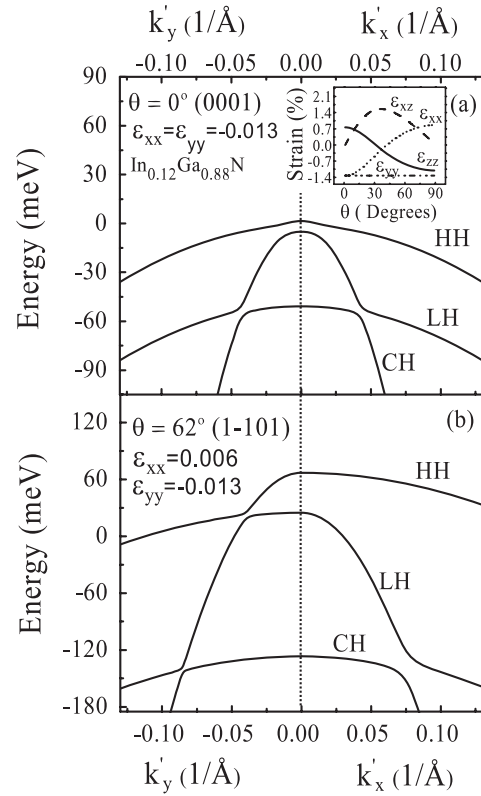

Figure 3. Valence band dispersion relations obtained by solution of the 6×6 **k · p** RSP Hamiltonian for two different wurtzite $In_{0.12}Ga_{0.88}N$ QW growth directions: (a) $\theta = 0°$ (0001) and (b) $\theta = 62°$ ($1\bar{1}01$). HH, LH and CH denote heavy-hole, light-hole and crystal-field split-off hole bands, respectively. The in-plane strain elements ε_{xx} and ε_{yy} are indicated. The inset in (a) illustrates the crystal orientation dependence of strain tensor elements. For $\theta > 0$, $\varepsilon_{xx} \neq \varepsilon_{yy}$ and the valence band profile becomes asymmetric in the k_x'–k_y' plane. We define the x, y, z crystallographic directions for c-plane (0001) growth in the usual manner, as [$1\bar{1}00$], [$11\bar{2}0$] and [0001], respectively.

range. A reversal of the strain induced behavior is observed for $\theta > 68°$. In figure 4(b) the strain induced variations in the bandgap of wurtzite $In_x Ga_{1-x}N$/GaN, ΔE_p, are plotted as a function of angle θ for various indium compositions in the $0.02 \leqslant x \leqslant 0.25$ range. ΔE_p is defined as the change in the bandgap relative to an unstrained $In_x Ga_{1-x}N$ film possessing the same indium composition x. For a given composition, x, the $In_x Ga_{1-x}N$/GaN bandgap has a maximum for $\theta = 0°$, the c-axis growth direction, and minimum for $\theta = 35°$, as indicated in figure 4(b). For $In_x Ga_{1-x}N$/GaN QW growth on the c-plane, ΔE_p increases linearly with the In composition and the in-plane compressive strain, as seen from figure 4(b). A reversal of this behavior is observed for $\theta > 12°$, where ΔE_p decreases almost linearly with the indium composition, reaching negative values, as seen from figure 4(b). This results in a strain induced decrease of the $In_x Ga_{1-x}N$/GaN bandgap for angles $\theta > 12°$, contrary to what is observed for QWs grown on the c-plane. This effect is especially pronounced for $\theta = 35°$.

In figure 4(c) the band-edge heavy-hole effective masses for dispersion along the k_x', k_y' and k_z' directions are plotted as
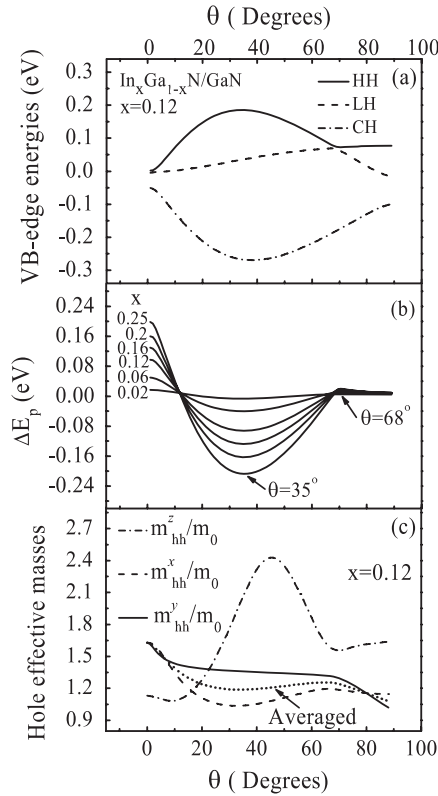
Figure 4. (a) Valence band-edge energies, (b) strain induced variations in the bandgap of the $In_xGa_{1-x}N/GaN$ quantum well structures of different In composition x and (c) effective heavy-hole masses (m_{hh}^z/m_0, m_{hh}^x/m_0 and m_{hh}^y/m_0) estimated from a parabolic band fitting to the calculated dispersion relations near the band edges as a function of angle θ between the QW growth direction $\hat{\mathbf{u}}(\theta)$ and the [0001] c-axis direction. HH, LH and CH denote heavy-hole, light-hole and crystal-field split-off hole bands, respectively. Heavy-hole effective-mass values that are averaged in the $k_x'-k_y'$ plane are indicated in (c) with a dotted line.

a function of angle θ for the strained layer $In_{0.12}Ga_{0.88}N/GaN$ system. The crystal orientation has ostensibly a strong effect on the in-plane and longitudinal heavy-hole effective masses, as seen from figure 4(c). Heavy-hole effective masses along the growth direction, m_{hh}^z, have a nonlinear dependence on θ, reaching a minimum for $\theta = 9°$ with $m_{hh}^z/m_0 = 1.07$ and a maximum for $\theta = 45°$ with $m_{hh}^z/m_0 = 2.45$. For $\theta > 0$, the in-plane asymmetry of the HH band structures results in a difference between heavy-hole effective masses along the k_x' and k_y' directions, i.e. $m_{hh}^x \neq m_{hh}^y$, as seen from figures 3(b) and 4(c). The averaged $k_x'-k_y'$ in-plane effective masses, that were used in our calculation of the exciton binding energies, are indicated in figure 4(c) with a dotted line. The average in-plane heavy-hole effective mass is significantly reduced with increasing angle θ, reaching its absolute minimum for $\theta = 90°$.

In figure 5(a), the strain induced piezoelectric (PZ) polarization ($P_z'^{pz}$) normal to the QW plane is plotted as a function of angle θ between the $In_xGa_{1-x}N/GaN$ QW growth direction and the c-axis direction for different In compositions in the $0.02 \leqslant x \leqslant 0.30$ range. The normal polarization leads to an accumulation or a depletion of carriers at the interfaces, creating the piezoelectric field in the QW. The
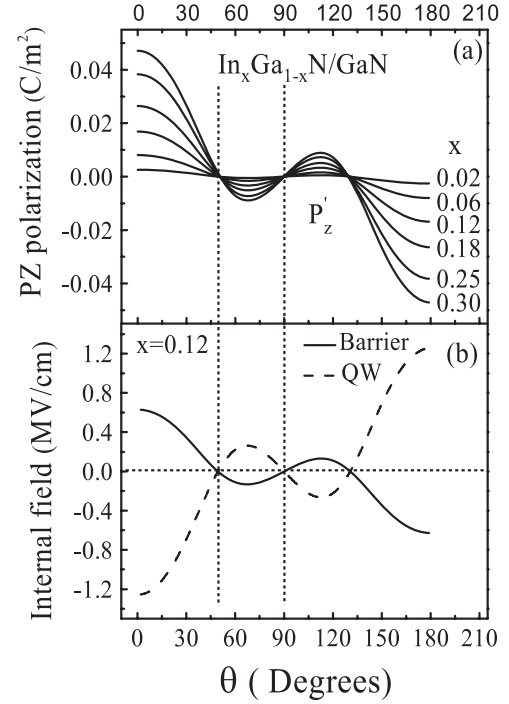

Figure 5. The strain induced piezoelectric polarization ($P_z'^{pz}$) normal with respect to the growth plane for $In_xGa_{1-x}N$ QWs of different In compositions x and (b) the internal field in the $In_{0.12}Ga_{0.88}N/GaN$ QW and adjacent barriers as a function of angle θ between the QW growth direction $\hat{\mathbf{u}}(\theta)$ and the c-axis. Vertical dotted lines emphasize growth directions corresponding to the zero PZ polarization and internal field.

normal polarization, $P_z'^{pz}$, is asymmetric with respect to the $[1\bar{1}00]$ growth direction ($\theta = 90°$), as seen from figure 5(a). The asymmetry of the normal polarization is due to the change of the atomic plane type (i.e. a cation versus anion termination) with respect to the $(1\bar{1}00)$ plane. For the [0001] c-axis QW growth direction $P_z'^{pz}$ is always positive for a compressive strain. The normal polarization shows a sign change with an increasing angle and becomes negative for θ in the $49.5° < \theta < 90°$ range, as observed in figure 5(a). Figure 5(b) shows the electric fields in an $In_{0.12}Ga_{0.88}N/GaN$ QW and adjacent GaN barrier as a function of angle θ, as calculated using our model approach. Vertical dotted lines emphasize the QW growth directions of $\theta = 49.5°$ and $90°$ (m-plane), corresponding to a zero piezoelectric polarization and electric field in the QW and the barrier.

3.2. Crystal orientation effects on properties of excitonic emission from InGaN/GaN QW

Figure 6 shows calculated probability distributions for the ground ($\Phi_{0(e-h)}\Phi_{0(e-h)}^*$) and first excited states ($\Phi_{1(e-h)}\Phi_{1(e-h)}^*$) of the heavy-hole excitons, along an arbitrary in-plane axis in $In_{0.12}Ga_{0.88}N/GaN$ QWs possessing different widths, (a) $L = 15$ nm and (b) $L = 1.5$ nm, grown on the $(1\bar{1}00)$-oriented m-plane ($\theta = 90°$). The in-plane exciton diameter, $2a_B^{xy}$, is indicated in figure 6(a) with vertical dotted lines. The exciton binding energy, E_B, and the in-plane exciton Bohr radius, a_B^{xy}, are 22.8 meV and 3.0 nm for $L = 15$ nm and 43.9 meV and 1.9 nm
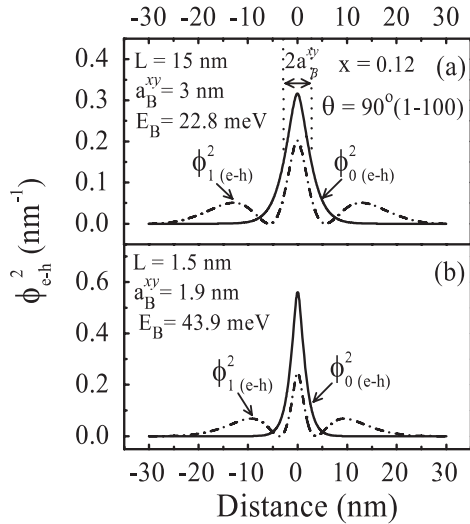
Figure 6. Probability densities for the ground ($\Phi_{0(e-h)}\Phi^*_{0(e-h)}$) and first excited states ($\Phi_{1(e-h)}\Phi^*_{1(e-h)}$) of the heavy-hole excitons, along an arbitrary in-plane axis in $In_{0.12}Ga_{0.88}N$/GaN QWs of different widths, (a) $L = 15$ nm and (b) $L = 1.5$ nm, grown on the ($1\bar{1}00$)-oriented m-plane ($\theta = 90°$). The in-plane exciton Bohr radius and the exciton binding energy are indicated for each QW width. The in-plane exciton diameter is indicated in (a) with vertical dotted lines.

Figure 7. (a) The exciton binding and transition energies, (b) the in-plane exciton radius and overlap integral of electron and hole envelope wavefunctions and (c) radiative lifetimes of free and localized heavy-hole excitons (X) at $T = 50$ K as a function of angle between the QW growth direction and the c-axis direction for a 3 nm thick $In_{0.12}Ga_{0.88}N$/GaN QW.

for $L = 1.5$ nm, respectively, as indicated in figures 6(a) and (b). The amplitude of the exciton ground-state wavefunction at the origin increases and the wavefunction becomes more localized as the width of the QW becomes smaller, owing to transition from a near 3D to a 2D quantum confinement as QW width decreases from $L = 15$ to 1.5 nm, as observed in figure 6. It should be mentioned here that $E_B = 22.8$ meV and $a_B^{xy} = 3.0$ nm obtained from our model calculation for QW width $L = 15$ nm are very close to the exciton binding energy and effective Bohr radius calculated for the bulk $In_{0.12}Ga_{0.88}N$ material: $E_B^{3D} = 21.8$ meV and $a_B^* = 3.02$ nm.

In figure 7, we show plots of the calculated exciton binding and transition energies, the in-plane exciton radius, the overlap integral of electron and hole envelope wavefunctions normal to the QW plane, and radiative lifetimes of free and strongly localized heavy-hole excitons for a 3 nm thick $In_{0.12}Ga_{0.88}N$/GaN QW as a function of angle θ. All orientation-dependent variations observed here, i.e. the increase of the exciton binding and transition energies as well as the decrease of the in-plane exciton radius and radiative lifetimes, which occur as the angle increases over the range $0 \leqslant \theta \leqslant 49.5°$, are primarily caused by decrease of the electric field in the QW. As seen from a comparison of figures 5 and 7, maxima (minima) of the electric field correlate well with calculated minima (maxima) of the exciton binding and transition energies and maxima (minima) of the in-plane exciton radius and radiative lifetime of excitonic emission. As previously mentioned, an increase of the electric field inside the QW results in a decrease of the overlap of electron and hole envelope wavefunctions normal to the QW plane and of the overlap integral, respectively, owing to the field-induced separation of the electron and hole wavefunctions towards
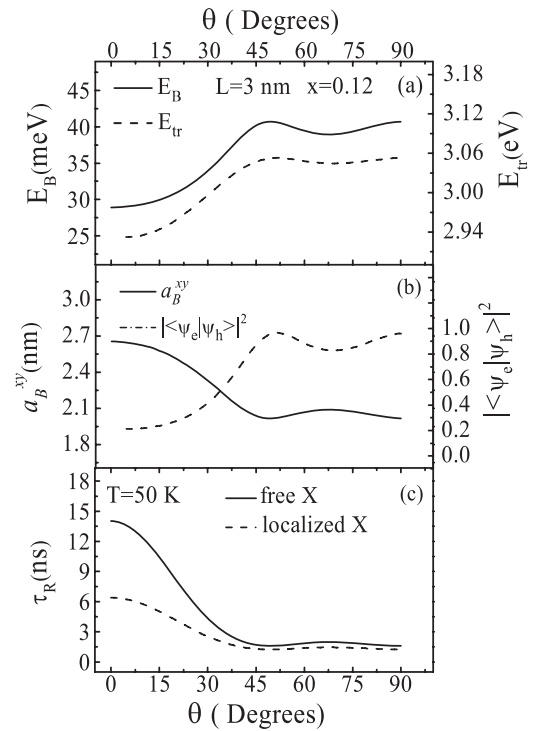
the opposite sides of the QW. The exciton binding energy is proportional to the oscillator strength, while the radiative lifetime is inversely proportional to the oscillator strength. For the free exciton with an in-plane wavevector $K_\perp = 0$, the oscillator strength Ω is well known and can be written as [53, 54]

$$\Omega = \Omega_0 k_0 n a_B^3 \Phi_{e-h}^2(0) I_{eh}^2 \qquad (19)$$

where Ω_0 and a_B are the bulk exciton oscillator strength and Bohr radius, n is the background refractive index, $k_0 = 2\pi/\lambda_{peak}$ is the wavevector of the photon at the excitonic resonance, I_{eh} is the overlap integral of electron and hole envelope wavefunctions normal to the QW plane and $\Phi_{e-h}^2(0)$ is the amplitude of the exciton ground-state wavefunction at the origin. An increase in the electric field inside the QW results in a decrease of the overlap integral of the electron and hole envelope wavefunctions, which according to equation (19) causes a decrease of the oscillator strength and the exciton binding energy and an increase of the radiative lifetime. For angles $\theta > \sim 49.5°$ only small variations on the order of $\sim 10\%$ in the exciton binding energies, transition energies and excitonic radiative lifetime are observed for narrow $In_{0.12}Ga_{0.88}N$/GaN QWs possessing widths less than ~ 3.5 nm. These results are illustrated for the case of a 3 nm thick QW in figures 7(a) and (c).

In figure 8 the exciton binding energies, the in-plane exciton radius and radiative lifetimes of strongly localized heavy-hole excitons are plotted as a function of
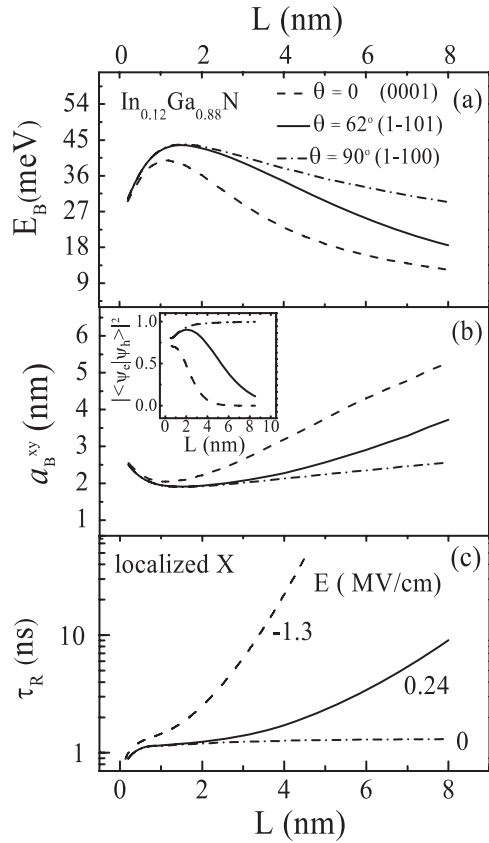
Figure 8. (a) Exciton binding energy, (b) in-plane exciton radius and (c) radiative lifetimes of localized heavy-hole excitons (X) as a function of the well width, L, for different $In_{0.12}Ga_{0.88}N/GaN$ QW growth directions ($\theta = 0°$, $62°$, and $90°$). The inset in (b) shows the overlap integral of electron and hole envelope wavefunctions versus well width L for different QW growth directions.

$In_{0.12}Ga_{0.88}N/GaN$ QW width for three different QW growth directions $\hat{\mathbf{u}}(\theta)$: $\theta = 0°$ (0001), $\theta = 62°$ ($1\bar{1}01$), and $\theta = 90°$($1\bar{1}00$). The exciton binding energies increase as the well width, L, becomes smaller, go through a maximum for $L = L_{max}$, and decrease when the electron and hole envelope wavefunctions normal to the QW plane start to penetrate into the barrier layers, as seen from figure 8(a). This is a well known behavior of a finite-barrier QW [49, 50]. Spreading of the electron and hole wavefunctions for $L < L_{max}$ results in a decrease of the overlap integral, shown in the inset of figure 8(b) for three QW growth directions, and leads to a decreased oscillator strength (see equation (19)) smaller binding energies, and larger in-plane exciton radii, as observed in figures 8(a) and (b). We observe that L_{max} (with E_B and a_B^{xy} at $L = L_{max}$) depends on the QW growth direction and varies from $L_{max} \approx 1.7$ nm (with $E_B = 43.9$ meV and $a_B^{xy} = 1.9$ nm) for QWs grown on the m-plane ($\theta = 90°$) with zero electric field inside the QW to $L_{max} \approx 1.1$ nm (with$E_B = 39.8$ meV and $a_B^{xy} = 2.05$ nm) for QWs grown on the c-plane ($\theta = 0$) with an electric field on the order of ~ 1.3 MV cm^{-1} in the QW region, as seen from figure 5.

The decrease of the exciton binding energy with increasing QW width obtained from our model for QWs grown on the m-plane can be attributed to the decrease

of the quantum confinement, owing to a transition from a 2D to a 3D case. The exciton ground-state wavefunction spreads out laterally in the QW plane, as the QW width becomes larger, which results in the increase of the in-plane exciton radius, and in the decrease in the amplitude of the exciton ground-state wavefunction at the origin, $\Phi_{e-h}^2(0)$, as seen from figure 6. According to equation (19) the decrease of $\Phi_{e-h}^2(0)$ results in a decrease of the oscillator strength and consequently a decrease of the exciton binding energy. Figure 8(c) shows a semi-logarithmic plot of radiative lifetimes of strongly localized heavy-hole excitons, τ_R, versus QW width for three different $In_{0.12}Ga_{0.88}N/GaN$ QW growth planes. For thin QWs we find radiative lifetimes in the range of several nanoseconds and almost independent of the QW growth direction. At the same time the QW growth direction has a strong effect on the radiative lifetimes for thicker QWs. As seen from figure 8(c), for QWs grown on the m-plane the radiative lifetimes are almost independent of the QW width, while for QWs grown on the c-plane the radiative lifetimes increase almost exponentially with the well width, owing to the field-induced decrease of the overlap integral, as seen from the inset in figure 8(b).

These trends reflect the often peculiar nature of fundamental excitonic parameters on the specific InGaN/GaN QW growth plane ($h\bar{h}0l$) and its direction $\hat{\mathbf{u}}(\theta)$. From these calculations, it is evident that a suitable choice of growth planes, such as the ($1\bar{1}01$) plane, will result in a radiative lifetime whose value is within a factor of two of the value of the radiative lifetime for an m-plane growth of $In_xGa_{1-x}N$ QWs possessing thicknesses $L \leqslant \sim 5$ nm. These results suggest that even a semi-polar plane such as ($1\bar{1}01$) can often be used to achieve QW characteristics that are similar to that for the non-polar m-plane over a practical range of $In_xGa_{1-x}N$ QW compositions and thicknesses. These observations are further consistent with the recent fabrication of highly efficient and bright LEDs on {$1\bar{1}01$} facets [18]. More recent time-resolved photoluminescence results of Wunderer et al have shown that InGaN/GaN QWs with $L \approx 4$ nm grown on {$1\bar{1}01$} semi-polar facets exhibit a drastically reduced lifetime of 650 ps at $T = 4$ K, in comparison to a reference QW grown on the c-plane, which exhibited a lifetime of 50 ns [19]. These experimental results are indeed consistent with our calculations of the radiative lifetimes for QWs grown on these planes, as shown in figure 8(c). The approaches and results described in this paper should help to stimulate further discussion on the appropriate choice of substrates and facets for the fabrication of $In_xGa_{1-x}N/GaN$ LDs and LEDs with optimal radiative quantum efficiencies.

4. Summary and conclusions

We have examined in detail crystal orientation effects on the properties of excitonic emission from wurtzite InGaN/GaN QWs with piezoelectric polarization using excitonic binding and transition energy calculations based on a single-band effective-mass theory. We have presented numerical results for the bandgaps, effective heavy-hole masses, piezoelectric polarizations and fields, exciton wavefunctions, exciton

binding energies, transition energies and radiative lifetimes of excitonic emission as a function of the QW growth direction. Band-edge and effective-mass parameters for a given QW growth direction $\hat{\mathbf{u}}(\theta)$ were obtained from In-composition- and strain-dependent $\mathbf{k} \cdot \mathbf{p}$ calculation for wurtzite $In_x Ga_{1-x}N$, using the 6×6 $\mathbf{k} \cdot \mathbf{p}$ Hamiltonian in appropriate $\{hkil\}$ representations. In particular, we examined the excitonic properties for InGaN/GaN QW growth on the technologically relevant family of $\{h\bar{h}0l\}$ planes. The excitonic ground- and first-excited-state energies and wavefunctions were calculated using an effective potential method. In this method the two-body exciton problem is reduced to a radial eigenequation involving the electron–hole relative motion in an effective in-plane Coulomb potential. The $In_x Ga_{1-x}N$ crystal orientation has a strong effect on the $In_x Ga_{1-x}N$ bandgap, the in-plane and longitudinal heavy-hole effective masses and piezoelectric polarization and electric field along the QW growth direction. The averaged in-plane heavy-hole effective mass decreases as θ changes from $\theta = 0°$ to $90°$. With increasing θ, the $In_x Ga_{1-x}N$ bandgap initially decreases, reaches a minimum for $\theta = 35°$ and increases again for larger angles. The piezoelectric polarization and field in the QW change their orientation twice for $\theta = 49.5°$ and $90°$. For these crystal growth directions, electric fields in the QW and barrier are equal to zero. The magnitude of the electric field in $In_x Ga_{1-x}N$/GaN QWs has a dominant effect on the transition energy and oscillator strength, which increase with angle θ, for $0 \leqslant \theta \leqslant 49.5°$, leading to a rapid increase in the exciton binding energy and decrease in the excitonic radiative lifetime. For angles $\theta > \sim 49.5°$, only small variations on the order of $\sim 10\%$ in the exciton binding energies, transition energies and excitonic radiative lifetime are observed for narrow $In_{0.12}Ga_{0.88}N$/GaN QWs that possess widths less than ~ 3.5 nm. These results indicate that InGaN/GaN QW materials grown on non-(0001)-oriented planes in a wide variety of angles $49.5° \leqslant \theta \leqslant 90°$ can be used for optimized operation of optoelectronic devices.

Acknowledgment

References

[1] Nakamura S, Mukai T and Senoh M 1991 *Japan. J. Appl. Phys.* **30** L1998
　　Nakamura S, Mukai T and Senoh M 1994 *Appl. Phys. Lett.* **64** 1687
[2] Nakamura S, Senoh M, Iwasa N and Nagahama S 1995 *Japan. J. Appl. Phys.* **34** L797
[3] Nakamura S, Senoh M, Nagahama S, Iwasa N, Yamada T, Matsushita T, Kiyoku H and Sigimoto Y 1996 *Appl. Phys. Lett.* **68** 2105
　　Nakamura S, Senoh M, Nagahama S, Iwasa N, Yamada T, Matsushita T, Kiyoku H and Sigimoto Y 1996 *Japan. J. Appl. Phys.* **35** L74
[4] Bykhovski A D, Kaminski V V, Shur M S, Chen Q C and Khan M A 1996 *Appl. Phys. Lett.* **68** 818
[5] Bernardini F, Fiorentini V and Vanderbilt D 1997 *Phys. Rev.* B **56** R10024

[6] Zoroddu A, Bernardini F, Ruggerone P and Fiorentini V 2001 *Phys. Rev.* B **64** 45208
[7] Chichibu S F, Azuhata T, Sota T and Nakamura S 1996 *Appl. Phys. Lett.* **69** 4188
　　Chichibu S F, Azuhata T, Sota T and Nakamura S 1997 *Appl. Phys. Lett.* **70** 2822
　　Chichibu S F, Azuhata T, Sota T and Nakamura S 1998 *Appl. Phys. Lett.* **73** 2006 and references therein
[8] Im J S, Kollmer H, Off J, Sohmer A, Scholz F and Hangleiter A 1998 *Phys. Rev.* B **57** R9435
[9] Miller D A B, Chemla D S, Damen T C, Gossard A C, Wiegmann W, Wood T H and Burrus C A 1984 *Phys. Rev. Lett.* **53** 2173
[10] Lefebvre P, Morel A, Gallart M, Taliercio T, Allegre J, Gil B, Mathieu H, Damilano B, Grandjean N and Massies J 2001 *Appl. Phys. Lett.* **78** 1252
[11] Deguchi T, Sekiguchi K, Nakamura A, Sota T, Matsuo R, Chichibu S and Nakamura S 1999 *Japan. J. Appl. Phys.* **38** L914
[12] Edmond J, Abare A, Bergman M, Bharathan J, Bunker K L, Emerson D, Haberern K, Ibbetson J, Leung M, Russel P and Slater D 2004 *J. Cryst. Growth* **272** 242
[13] Ng H 2002 *Appl. Phys. Lett.* **80** 4369
[14] Craven M, Waltereit P, Wu F, Speck J and DenBaars S 2003 *Japan. J. Appl. Phys.* 2 **42** L235
[15] Imer B M, Wu F, DenBaars S P and Speck J S 2006 *Appl. Phys. Lett.* **88** 061908
[16] Waltereit P, Brandt O, Trampert A, Grahn H, Menniger J, Ramsteiner M, Reiche M and Ploog K 2000 *Nature* **406** 865
[17] Nishizuka K, Funato M, Kawakami Y, Fujita S, Narukawa Y and Mukai T 2004 *Appl. Phys. Lett.* **85** 3122
[18] Wunderer T, Brückner P, Neubert B, Scholz F, Feneberg M, Lipski F, Schirra M and Thonke K 2006 *Appl. Phys. Lett.* **89** 041121
[19] Wunderer T, Brückner P, Hertkorn J, Scholz F, Beirne G J, Jetter M, Michler P, Feneberg M and Thonke K 2007 *Appl. Phys. Lett.* **90** 171123
[20] Schwarz U T and Kneissl M 2007 *Phys. Status Solidi* **1** A44–6
[21] Chakraborty A, Baker T J, Haskell B A, Wu F, Speck J S, DenBaars S P, Nakamura S and Mishra U K 2005 *Japan. J. Appl. Phys.* **44** L945
[22] Funato M, Ueda M, Kawakami Y, Narukawa Y, Kosugi T, Takahashi M and Mukai T 2006 *Japan. J. Appl. Phys.* **45** L659
[23] Chakraborty A, Haskell B A, Keller S, Speck J S, DenBaars S P, Nakamura S and Mishra U K 2005 *Japan. J. Appl. Phys.* **44** L173
[24] Feneberg M, Lipski F, Sauer R, Thonke K, Wunderer T, Neubert B, Brückner P and Scholz F 2006 *Appl. Phys. Lett.* **89** 242112
[25] Park S-H and Chuang S-L 1999 *Phys. Rev.* B **59** 4725
[26] Park S-H 2000 *Japan. J. Appl. Phys.* **39** 3478
　　Park S-H 2002 *J. Appl. Phys.* **91** 9904
　　Park S-H 2003 *J. Appl. Phys.* **93** 9665
[27] Fiorentini V, Bernardini F, Della Sala F, Di Carlo A and Lugli P 1999 *Phys. Rev.* B **60** 8849
[28] Takeuchi T, Amano H and Akasaki I 2000 *Japan. J. Appl. Phys.* **39** 413
[29] Khatsevich S, Rich D H, Zhang X, Zhou W and Dapkus P D 2004 *J. Appl. Phys.* **95** 1832
[30] Khatsevich S, Rich D H, Zhang X and Dapkus P D 2007 *J. Appl. Phys.* **102** 093502
[31] Feneberg M and Thonke K 2007 *J. Phys.: Condens. Matter* **19** 403201
[32] Minsky M S, Fleischer S B, Abare A C, Bowers J E, Hu E L, Keller S and Denbaars S P 1998 *Appl. Phys. Lett.* **72** 1066

[33] Kim H J, Na H, Kwon S-Y, Seo H-C, Kim H J, Shin Y, Lee K-H, Kim Y-W, Yoon S, Oh H J, Sone C, Park Y, Cho Y-H, Sun Y and Yoon E 2003 *Phys. Status Solidi* c **0** 2834
[34] Kunold A and Pereyra P 2003 *J. Appl. Phys.* **93** 5018
[35] Shan W, Little B D, Song J J, Feng Z C, Shurman M and Stall R A 1996 *Appl. Phys. Lett.* **69** 3315
[36] Voznyy A V and Deibuk V G 2004 *Semiconductors* **38** 304
[37] Lefebvre P, Kalliakos S, Bretagnon T, Valvin P, Taliercio T, Gil B, Grandjean N and Massies J 2004 *Phys. Rev.* B **69** 035307
[38] Kalliakos S, Lefebvre P and Taliercio T 2003 *Phys. Rev.* B **67** 205307
[39] Christmas U M E, Andreev A D and Faux D A 2005 *J. Appl. Phys.* **98** 073522
[40] Wu J-W 1989 *Solid State Commun.* **69** 1057
[41] Sirenko Y M, Jeon J–B, Kim K W, Littlejohn M A and Stroscio M A 1996 *Phys. Rev.* B **53** 1997
[42] Chuang S L and Chang C S 1996 *Phys. Rev.* B **54** 2491
[43] Park S H and Chuang S L 1999 *Phys. Rev.* B **59** 4725
    Park S H and Chuang S L 2002 *Semicond. Sci. Technol.* **17** 686
    Park S H and Chuang S L 1998 *Appl. Phys. Lett.* **72** 3103
    Park S H and Chuang S L 2000 *Appl. Phys. Lett.* **76** 1981
[44] Hinckley J M and Singh J 1990 *Phys. Rev.* B **42** 3546
[45] Smith D L and Mailhiot 1988 *J. Appl. Phys.* **63** 2717
[46] Bykhovski A, Gelmont B and Shur S 1993 *Appl. Phys. Lett.* **63** 2243
[47] Leroux M, Grandjean N, Massies J, Gil B, Lefebvre P and Bigenwald P 1999 *Phys. Rev.* B **60** 1496
[48] Bastard G, Mendez E E, Chang L L and Esaki L 1982 *Phys. Rev.* B **26** 1974
[49] Greene R L and Bajaj K K 1983 *Solid State Commun.* **45** 831
[50] Greene R L, Bajaj K K and Phelps D E 1984 *Phys. Rev.* B **29** 1807
[51] Lefebvre P, Allegre J, Gil B, Kavokine A, Mathieu H, Kim W, Salvador A, Botchkarev A and Morkoc H 1998 *Phys. Rev.* B **57** R9447
[52] Khatsevich S, Rich D H, Keller S and DenBaars S P 2007 *Phys. Rev.* B **75** 035324
[53] Citrin D S 1992 *Solid State Commun.* **84** 281
    Citrin D S 1993 *Phys. Rev.* B **47** 3832
    Citrin D S 1993 *Superlatt. Microstruct.* **13** 303
[54] Andreani L C and Bassani F 1990 *Phys. Rev.* B **41** 7536